Article

Order−Disorder Transition in Rutile VO₂(M) Electrodes during Li Intercalation and Extraction

Morten Johansen and Dorthe B. Ravnsbæk*

Cite This: *ACS Omega* 2024, 9, 36291−36298
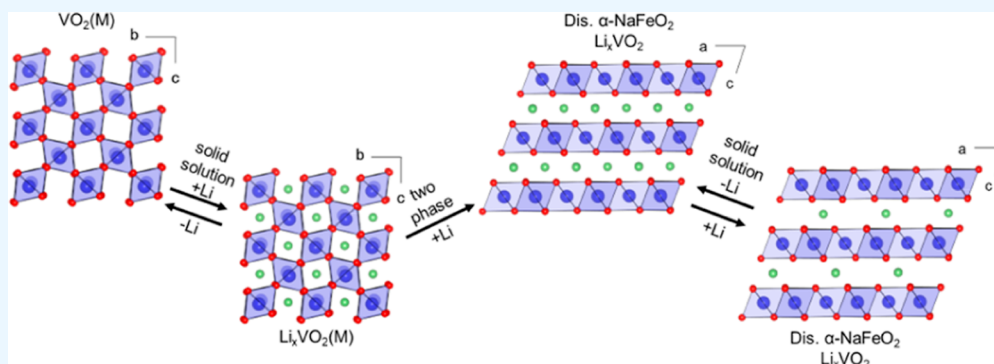
Read Online

ACCESS | 📊 Metrics & More | 📖 Article Recommendations | 🔷 Supporting Information

ABSTRACT: Transition metal oxides are widely employed as electrode materials in Li-ion batteries. During battery operation, Li ions are intercalated and extracted from the framework of the electrode structure, causing structural transitions. In some materials, the process can drive order−disorder transitions; however, insights into such processes are generally lacking, although they are essential for our understanding of battery aging and in the design of new sustainable battery chemistries. Herein, we investigate the intercalation-induced order−disorder transition in rutile $VO_2(M)$ electrodes by means of galvanostatic charge/discharge cycling, *operando* powder X-ray diffraction, and total X-ray scattering with pair distribution function analysis. The study reveals that the rutile structure transforms irreversibly into a highly disordered layered Li_xVO_2 structure, which is capable of reversibly intercalating Li ions. Our findings point out general trends for the intercalation-driven transitions in rutile oxides.

INTRODUCTION

Rechargeable Li-ion batteries (LIB) are widely used for electrochemical energy storage and promote the transition toward a more sustainable energy system. As a result of the continuously growing demand for LIB, novel chemistries and enhanced understanding of the energy conversion mechanism are constantly sought.[1−3] Within this frame, understanding the structural transitions occurring within the electrodes during battery charge and discharge is an important aspect that relates directly to battery performance. The focus has traditionally been on crystalline-to-crystalline phase transitions between the lithiated and delithiated states of the electrode material. However, many electrodes undergo varying degrees of order−disorder transitions during battery cycling.[4,5] Structural disorder or complete amorphization can have a destructive effect on the ion-intercalation and lead to severe capacity fade.[5,6] On the other hand, some reports also show that lack of long-range order can improve the battery performance and even exceed the performance of the crystalline analogue.[7,8]

Transition metal oxides are well-known and established electrode materials for rechargeable LIB, which offer a variety of possibilities for variation both in composition and polymorphism.[9] The layered transition metal oxides,

$LiTMO_2$, represent the most widely employed and studied positive electrode material for LIB. For this class of material, the Li-ion deintercalation and reintercalation processes can lead to structural disorder in the form of stacking faults, transition metal migration, and so on.[10−13] However, the crystalline lattice generally remains intact. More extensive disorder is observed during intercalation in other transition metal oxides. One example is rutile titanium oxide, TiO_2, which undergoes a phase transitions as a result of Li-ion intercalation into a disordered layered α-NaFeO₂-like $LiTiO_2$ with a coherence length of ∼5 nm separated by ∼1 nm thick grain boundary with a columbite-like structure.[6]

To extend the knowledge of phase transitions during Li-ion interaction in rutile-like transition metal oxides, we herein investigate the case of the rutile-like vanadium oxide
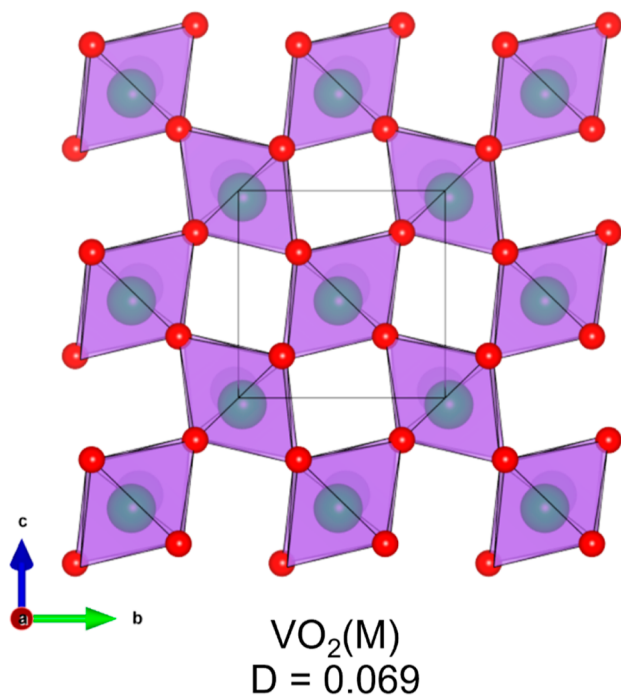
polymorph, $VO_2(M)$. $VO_2(M)$ crystallizes in the monoclinic space group $P2/c$,[14] and the structure of $VO_2(M)$ is built from chains of corner sharing $[VO_6]$ octahedra running along the a-axis and connected by corner sharing in the bc-plane (Figure 1). The monoclinic $VO_2(M)$ was first described in the

Figure 1. Crystal structure of monoclinic $VO_2(M)$ with distortion index, D, of the $[VO_6]$ octahedra.

literature as a deformed rutile by Andersson in 1956, where he stated that $VO_2(M)$ was "···built up of distorted VO_6 octahedra joined by edges to form strings, which are mutually connected by corners to a three-dimensional network of deformed rutile type".[15] $VO_2(M)$ has been studied as a potential electrode material for rechargeable LIB, which due to the 1D-tunnel structure and low mass exhibits efficient lithium diffusion and high theoretical capacity.[16,17] $VO_2(M)$ has a theoretical gravimetric capacity of 320 mA h/g, however prior studies have presented low reversible capacities due to the anisotropic accommodation of lithium ions.[18,19] Such studies have deemed $VO_2(M)$ unsuitable as an electrode for rechargeable LIB. Most studies report an irreversible phase transition at higher levels of lithiation, in accordance with rutile structures undergoing a crystalline to disorder phase transition.[20,21]

To investigate the structural transitions induced by Li-ion intercalation in $VO_2(M)$ electrodes, the pristine crystalline phase and the fully lithiated highly disordered phase are studied herein using powder X-ray diffraction (PXRD) and total X-ray scattering (TXS) with pair distribution function (PDF) analysis. To gain insight into the true dynamic process of structural changes, X-ray experiments were conducted under *operando* conditions during galvanostatic discharging /charging. By combining the information extracted from the measurements, we provide a structural description of the phase transitions during the first Li intercalation and extraction into $VO_2(M)$.

■ EXPERIMENTAL SECTION

Solvothermal Synthesis of $VO_2(M)$. $VO_2(M)$ was synthesized similar to the description by Corr *et al.*[22] In an 80-mL Teflon-lined autoclave containing a Teflon-lined stirring bar, 1.81 g of vanadium(V) pentoxide (≥99.6%, Sigma-Aldrich) was suspended in 30 mL of formaldehyde (37 wt % in H_2O, stabilized with 5−15% methanol, Acros Organics) and left under magnetic stirring. After 2 h of stirring, the autoclave, containing the red suspension, was sealed and heated at 180 °C for 48 h. The resulting blue powder, $VO_2(B)$, was filtered and washed with ethanol (96%, Sigma-Aldrich) and demineralized water through suction filtration and left to dry overnight under vacuum at 60 °C. After drying the powder was grinded using mortar and pestle and transferred to an alumina (Al_2O_3) crucible. The powder was heated at 300 °C/h and annealed at 700 °C for 1 h followed by cooling to room temperature. At room temperature, the powder was transferred and stored in an Ar-filled glovebox.

Chemical Lithiation. This process was conducted in an Ar-filled glovebox. 0.205 g of the prepared $VO_2(M)$ was transferred to a 50-mL Erlenmeyer flask and suspended in 20 mL dry n-heptane (+99%, extra dry over molecular sieves, Acros Organics). To this suspension was added 0.920 mL of a 2.7 M solution of n-butyllithium in hexane (Sigma-Aldrich) slowly using a dry 1 mL plastic syringe equipped with a metal needle. The flask was equipped with a screw cap and left to react for 24 h under magnetic stirring. The following day the liquid was decanted and washed with n-heptane (+99%, extra dry over molecular sieves, Acros Organics), and the powder was left to dry under an Ar-atmosphere.

Electrochemical Characterization. The as-synthesized $VO_2(M)$ powder was mixed with acetylene black (VXC72, Cabot Corporation), graphite (C-NERGY SFG6L, IMERYS) and polyvinylidene fluoride binder (HSV900, MIT) in a 6:1:1:2 mass ratio dispersed in acetone for thorough mixing. The mixture was dispersed onto a glass plate and scraped off to isolate the electrode pellet mixture. The pellet mixture was pressed into Ø 7-mm free-standing pellets, weighing between 5 and 8 mg, under a uniaxial press at 1.8 t for 60 s and dried at 60 °C under vacuum overnight. Galvanostatic cycling was performed using a Swagelok type cell with a Teflon body. A cathode pellet was mounted on a stainless-steel cylinder with Ø 11-mm lithium metal foil serving as the anode. To separate the electrodes, a microporous, Whatman GF/B, glass fiber wetted with electrolyte was used. A 1 M solution of lithium hexafluorophosphate ($LiPF_6$, Solvionic, 99.9%, ethylene carbonate/dimethyl carbonate 1:1, v/v) worked as electrolyte. These batteries were cycled between 1.0 and 4.0 V against Li/Li$^+$ using a Biologic VMP-3 battery cycler. The number of intercalated Li-ions, x, is based on Coulomb counting, assuming all current goes into Li-ion intercalation.

X-Ray Diffraction and Total Scattering. Samples for *ex situ* X-ray total scattering (TXS) and powder diffraction (PXRD) were measured in polyimide Kapton capillaries (Ø 1.0-mm inner diameter, Cole-Parmer). All measurements were taken at the P02.1 beamline at PETRA III at DESY, Germany, using synchrotron radiation. The data were measured with a wavelength of 0.20735 Å using a Varex XRD 4343CT (150 × 150 μm^2 pixel size, 2880 × 2880 pixel area) detector. PXRD measurements were all obtained within 30 s of exposure, and the Kapton capillaries were spun. PDF samples were measured

with 50 s exposure and 40 subframes in *ex situ*, while *operando* was measured using 60 s exposure and four subframes. For *operando* PXRD and PDF experiments, the cathode pellet was mounted in an AMPIX-type battery test cell and cycled at C/12. *Operando* PXRD data were collected every 8 min while PDF data were collected every 30 min.

Both PXRD and PDF was calibrated using either a NIST CeO_2 or a LaB_6 standard placed at the sample position in either Kapton capillaries or in the AMPIX cell. Single-crystal spots from the lithium metal anode were masked before the data was calibrated and integrated using the Data Analysis WorkbeNch (DAWN)[23] software. Corrections for fluctuations in the beam were done with a normalization of the data background at low Q or 2θ values.

The data were normalized to correct for fluctuations in beam intensities over a range of background points at low 2θ or Q [$Q = 4\pi \sin(\theta)\lambda^{-1}$]. Rietveld refinement was conducted using the FullProf suite[24,25] for both *operando* and *ex situ* PXRD. The PDFgetX3[26] was used to obtain PDF's from the TXS data with an r_{poly} set to 0.9 Å and Q_{max} values of 23.3 and 28.0 Å^{-1} for *operando* and *ex situ*, respectively. PDF-fits were done with the PDFgui software.[27] All crystal structures are made using VESTA.[28] The distortion index, *D*, of the [VO_6] octahedra are calculated from eq 1 using VESTA, with *n* as the number of V–O bonds, l_i, the length of the *i*th V–O bond and l_{av} being the average V–O bond length.

$$D = \frac{1}{n} \sum_{n=i}^{n} \frac{|l_i - l_{av}|}{l_{av}}$$ (1)

■ RESULTS AND DISCUSSION

Characterization of the As-synthesized VO_2(M). The expected monoclinic rutile-like VO_2(M) phase was obtained from the solvothermal synthesis and subsequent solid-state treatment as confirmed by PXRD and Rietveld refinement (Figure 2). PXRD also reveals the presence of a small amount of nanocrystalline VO_2(B) in the sample (see broad and low intensity reflections at 1.81 and 3.95 Å^{-1}). Refinement of the PDF (Figure 2B) obtained from a total scattering experiment (Table S2) confirms both the structural model of VO_2(M) as obtained from Rietveld refinement (Table S1) and the presence of a small amount of VO_2(B).

Electrochemical Characterization of VO_2(M) Electrodes. During the first discharge (Figure 3A), ~0.94 Li is inserted into VO_2(M) when cycling versus Li-metal at a C/12-current rate to a lower cutoff potential of 1.0 V. A plateau is observed for the intercalation just below 2.0 V. Inspection of the first derivative of the discharge curve reveals that there might be separate discharge domains. Hence, for $x < 0.04$, the sloping nature is likely originating from a direct response of the polarization and diffusion-induced resistance effects.[29] The domain at $0.04 < x < 0.18$ may originate from the effect of a constantly changing crystal structure as observed in a typical solid solution transition. At $x \sim 0.15-0.35$ Li-ions, the potential profile shows features that could indicate an overlap between solid solution behavior and a biphasic transition. At $x \sim 0.35 > x > 0.75$ Li-ions, the first derivative is almost constant at zero, suggesting a biphasic transition occurring at this point. For the remaining discharge, the curve slope increases, which may indicate solid solution behavior and beyond $x \sim 0.8$ polarization comes into play.
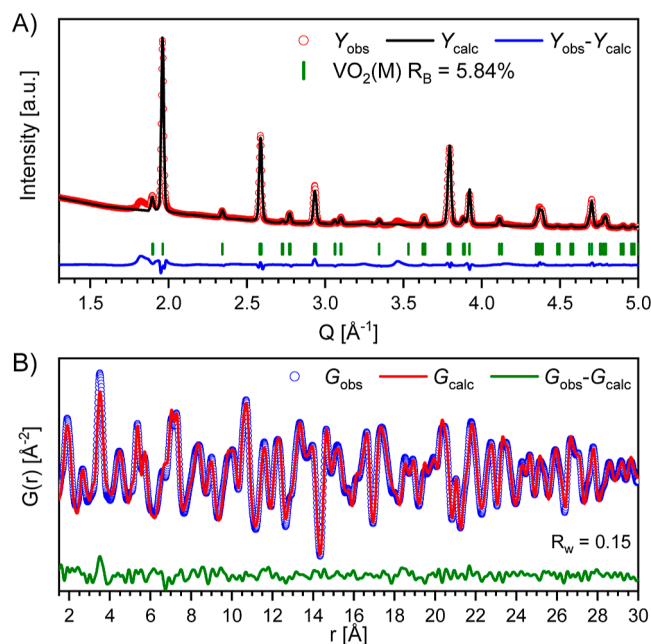
Figure 2. Structural characterization of the as synthesized VO_2(M) by (A) PXRD with Rietveld refinement, and (B) PDF with refinement. Results from the refinements is found in Tables S1 and S2.
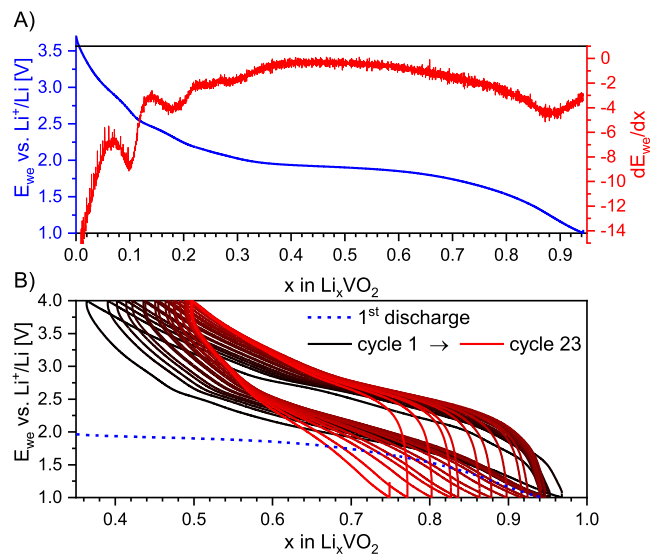

Figure 3. (A) Potential profile (blue) and first derivative (red) of the first galvanostatic discharge of VO_2(M) versus Li metal. (B) Potential profiles for repeated galvanostatic discharge/charge cycling of VO_2(M) versus Li metal.

From the profiles from the repeated galvanostatic discharge/charge cycling (Figure 3B), it is evident that the first discharge differs significantly from the following cycles. First, the plateau is lost upon cycling, indicating increasing solid solution behavior with cycling. Furthermore, looking beyond the first discharge, it becomes clear that the system slowly loses capacity.

***Operando* PXRD.** To gain insight into the structural evolution of VO_2(M) electrode during Li-ion intercalation, *operando* PXRD (Figure 4) was collected during galvanostatic cycling *vs* a Li-metal anode in an AMPIX cell.

During insertion of the first ~0.25 Li, the Bragg reflections from Li_xVO_2 are well-defined and only minor structural
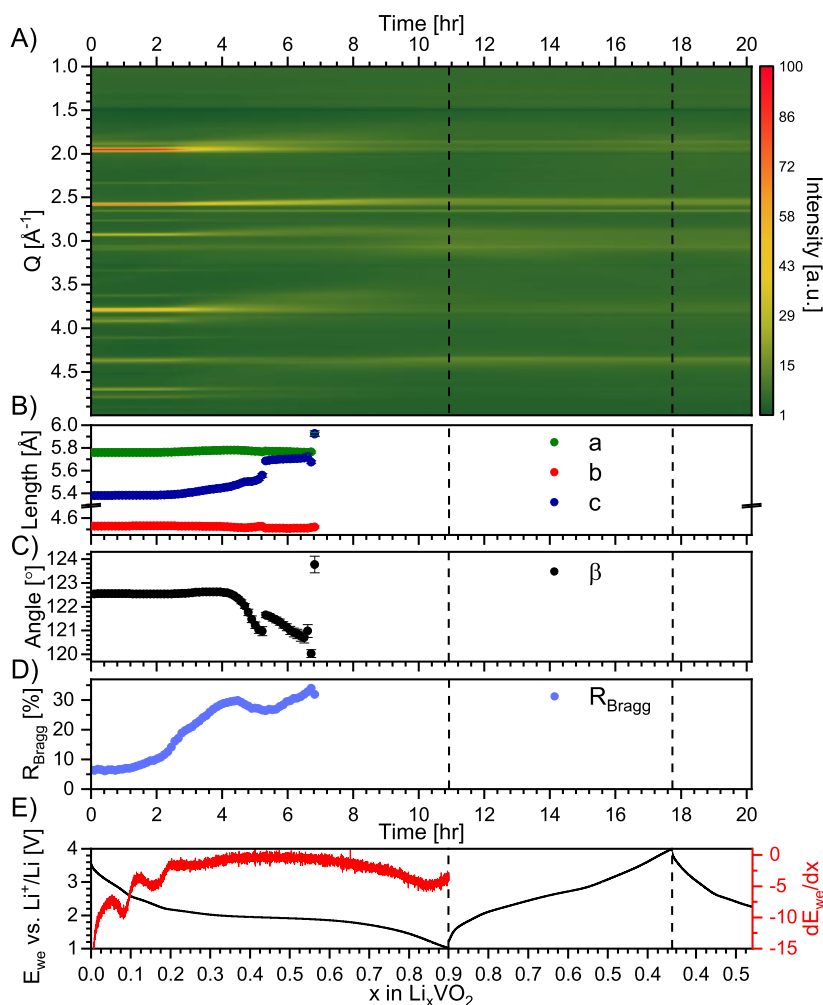
Figure 4. (A) *Operando* PXRD data plotted as a function of time and x in Li_xVO_2. The weak reflection at 2.565 $Å^{-1}$ is caused by the Li-metal anode. (B,C) Refined lattice parameters for $Li_xVO_2(M)$ for the first 65 scans after which the Rietveld method can no longer describe the data satisfactorily, which is also reflected in the agreement factor, R_{Bragg}, in (D). (E) Potential and first derivative as a function of x in Li_xVO_2 during discharge and charge against a Li-metal anode at a C/12-current rate.

changes occur with a slight expansion in the *c*-direction. Upon continued Li insertion, the *c*-axis continues to expand; however, the intercalation causes the Bragg reflections to gradually diffuse, and the Rietveld model provides an increasingly poor description of the data suggesting loss of crystallinity due to disordering. As an electrode composition of $Li_{\sim 0.4}VO_2$ is reached, the Rietveld refinement model becomes unreliable reflected in the sudden shift in the refined values for the *c*-axis and the β-angle. At $Li_{\sim 0.5}VO_2$ the model fails and is no longer able to describe the system, that is the degree of crystallinity in $Li_{0.5}VO_2$ is too low to allow for quantitative analysis by PXRD. During this process, no new sharp Bragg reflections appear, and beyond insertion of 0.5 Li only weak and diffuse reflections are observed. Hence, the Li-intercalation drives an order−disorder transition. The observed behavior bears strong resemblance to the rutile Li_xTiO_2 system.[6] In the TiO_2 system, Christensen *et al.*[6] report that upon continues Li-insertion above $Li_{0.78}TiO_2$, the system rearrange into ∼5 nm domains of a layered α-$NaFeO_2$ structure with small amounts of amorphous Li_xTiO_2 columbite. Based on this knowledge, it is possible to describe the scattering data beyond 0.5 Li using Le Bail fitting with unit cells resembling a layered α-$NaFeO_2$ (space gr. $P2/m$, no. 10) and a columbite (space gr. $Pbcn$, no.

60) structures (Figure S3).[6] From the *operando* PXRD data (Figure 4) it is also clear that rutile $Li_xVO_2(M)$ is not reformed during charge and that the material remains in the disordered state with a structure resembling the structure of the discharge state, *i.e.* the disordered layered α-$NaFeO_2$ and columbite structures behaves as solid solutions toward Li-ion intercalation.

Characterization Using Total Scattering with Pair Distributions Function Analysis. To get insight into the atomic structure of Li_xMO_2 at $x > 0.5$, a $VO_2(M)$ sample was chemically lithiated using *n*-butyllithium and the PDF of this was obtained *ex situ* (Figure 5). This sample provides a higher quality PDF as compared to the functional electrode, which, besides the active materials, also contains binder and carbon additives. Fitting the PDF of chemically lithiated sample shows that most correlations can be explained by a $LiVO_2$ structure with a distorted α-$NaFeO_2$-structure as in the Le Bail fit. However, the fit clearly improves by addition of a VO_2 columbite phase, especially in the lower *r* region ($r < 10$ Å). Based on the agreement factors and the shape of the residual other minor phases may be present as well. We note that lithiated $LiVO_2(M)$ and $LiVO_2(B)$ structure were also tested as both the major and minor phase; however, these did not
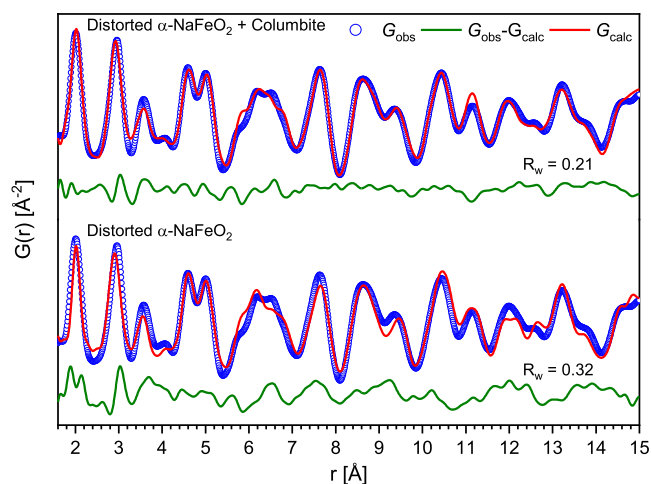
Figure 5. PDF fits of chemical lithiated $Li_{x\sim1}VO_2(M)$ showing a clear improvement in the residual when including both a distorted α-NaFeO$_2$ and columbite models. Fitted parameters are found in Tables S3 and S4.

provide good fits to the data. Hence, from the *ex situ* PDF we confirm that rutile-like $VO_2(M)$ upon lithiation transforms to a layered $LiVO_2$ structure (Figure 6) as observed for rutile TiO_2. DFT calculations by Kulish *et al.*[30] suggests that lithium ions are intercalated into the octahedral sites in the rutile structure as this is energetically more favorable than the tetrahedral sites. By filling up the octahedral sites the structure approaches an NiAs structure (hcp packing of oxygen with all octahedral holes filled), which is rarely observed for stoichiometric oxides.[6] Hence, the irreversible structural rearrangement occurs wherein the oxygen lattice rearranges to a ccp packing, which can accommodate full occupancy on all octahedral sites (*i.e.*, rock salt structure). For the structure to transform from rutile- to α-NaFeO$_2$-like (*i.e.*, to become layered), the V atoms in every second layer in $VO_2(M)$ must translate 0.5 along the *c*-axis. It is plausible that this translation only occurs for a part of the V atoms and that Li and V instead are distributed over all octahedral sites (*i.e.*, rock salt structure). However, fitting a structural model with varying amounts of V on the Li-positions

in the layered α-NaFeO$_2$-like $LiVO_2$ structure does not improve the fit. This is also evident from comparison of calculated PDFs from the layered α-NaFeO$_2$-like $LiVO_2$ structure and the rock salt like $LiVO_2$ structure (Figure S4). Hence, after chemical lithiation, the $LiVO_2$ appears to truly have a layered structure. Note that in the α-NaFeO$_2$-like $LiVO_2$ structure, there are only edge-sharing and no corner sharing $[VO_6]$ octahedra. Columbite has a high $[VO_6]$ corner-to-edge-sharing ratio of 3.5. Hence, the improvement of the PDF fit obtained from adding a local columbite phase reveals that a fraction of the material still contains corner sharing $[VO_6]$.

To follow the dynamic changes in the local atomic structure, an *operando* TXS measurement was performed during discharge and charge of the $VO_2(M)$ electrode versus Li. From here, the *operando* PDF data was obtained. The PDF confirms that the coherence length significantly decreases with insertion of Li (see Figure S2) and that structural order is only observed on the local scale ($r < 30$ Å) in the lithiated state. Hence, an PDF overview plot of the local structure and simulated PDFs for the relevant phases is shown together with the galvanostatic discharge/charge curve in Figure 7. Note that the carbon windows of the AMPIX cell and carbon additives in the electrode give rise to correlations at ~1.4, ~2.5, ~2.8, ~3.8 and ~4.4 Å.

By visual inspection of the *operando* PDF data, it is clear that some changes in the local atomic structure are induced by battery cycling. A gradual shift in the correlations is observed already at the very early stages of Li-intercalation, which may suggest that Li-ions are intercalated into $VO_2(M)$ *via* a solution solid reaction in line with the observation of continuous changes to the lattice parameters in the *operando* PXRD data.

Looking at interatomic distances in the observed phase (Figure 6), we see that the V−O distances in the $[VO_6]$ octahedra in $VO_2(M)$ are 1.7−2.1 Å, while in $LiVO_2$ they are 2.0−2.1 Å, that is, in average slightly longer in line with the reduction of V^{4+} to V^{3+}. The data clearly show that the $[VO_6]$ is not broken or heavily distorted at any point. The shortest V−V distance appears between the edge-sharing $[VO_6]$ octahedra. In $VO_2(M)$ this is ~2.60 Å, while it is ~2.95 Å
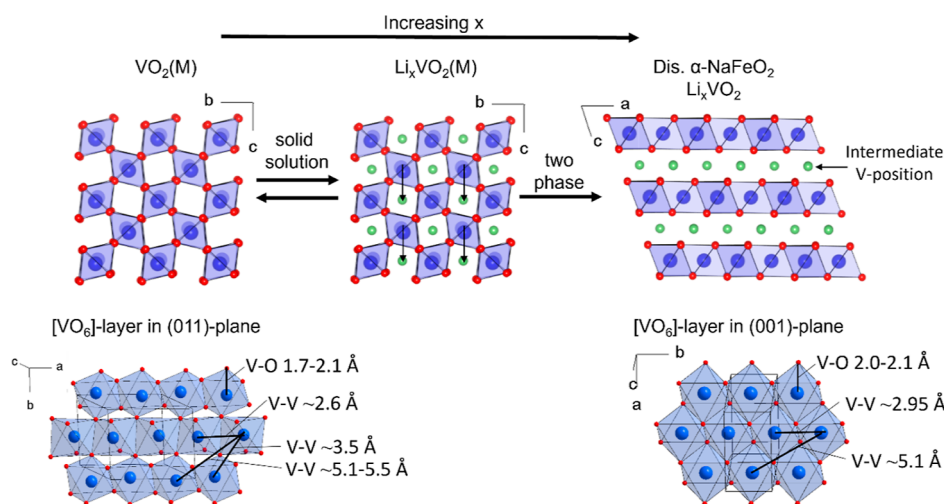
Figure 6. Illustration of the observed phase transition during first lithiation/discharge. For the endmembers $VO_2(M)$ and Li_xVO_2, the layers of $[VO_6]$-octahedra are shown along with interatomic distances of importance for the *operando* PDF analysis. V is shown in blue, O in red, and Li in green.
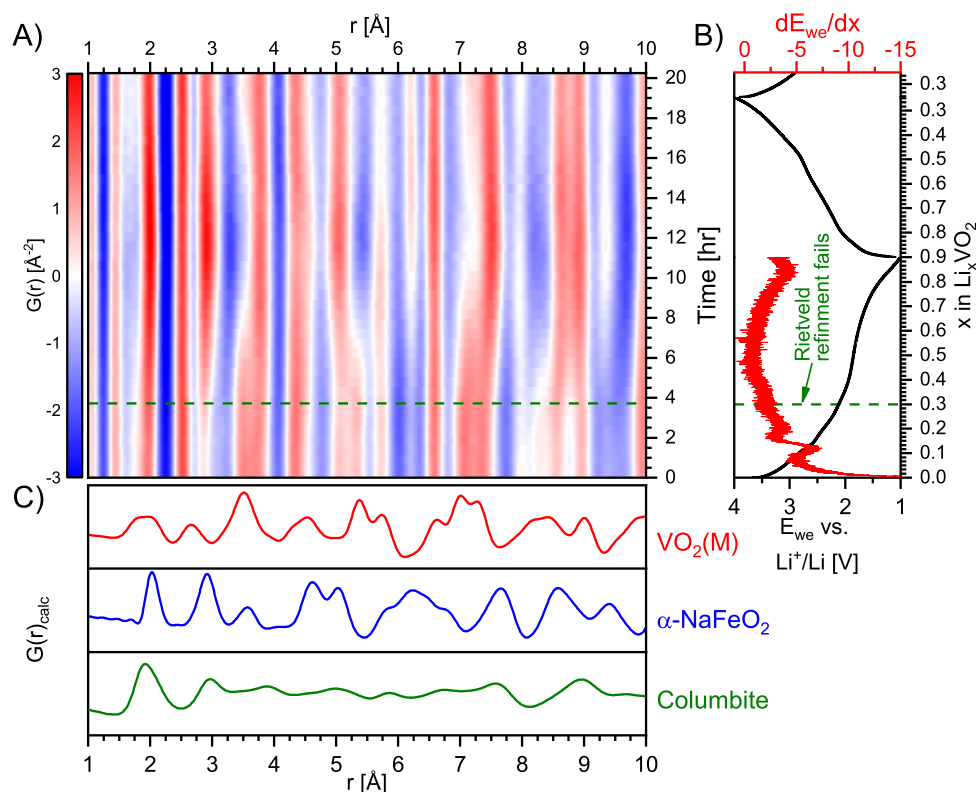
Figure 7. (A) Overview plot of the *operando* PDFs plotted as a function of time and x in Li_xVO_2 during galvanostatic cycling of $VO_2(M)$ versus Li metal anode at a C/12 rate. (B) The potential profile (black) for the first discharge is plotted with the first derivative (red) to enhance the electrochemical domains. (C) Calculated PDFs of pristine $VO_2(M)$, the distorted α-$NaFeO_2$, and columbite phases are shown underneath the overview plot for comparison.

in $LiVO_2$. The latter correlation emerges after insertion of ~0.2 Li and just before Rietveld refinement of the PXRD fails (Figure 4). From $VO_2(M)$, strong correlations are observed at ~3.5 and 5.1–5.5 Å, originating from the distance between V atoms in the adjacent $[VO_6]_n$ chains running along the *a*-axis. These correlations fade during lithiation, and upon insertion of ~0.6 Li they have vanished as seen from Figure 7. Instead, a strong correlation appears at ~5.1 Å due to V–V distances in the layers of edge sharing $[VO_6]$ octahedra forming in $LiVO_2$. Hence, these observations confirm that the number of corner sharing $[VO_6]$ octahedra as found in rutile decreases on the expense of edge sharing $[VO_6]$ octahedra as found in α-$NaFeO_2$. We note that the correlations indicative of $VO_2(M)$ do not reappear upon charge, that is, $VO_2(M)$ does reform neither in a crystalline nor in an amorphous state.

Turning our attention to the charge process, we find that the charged state resembles the discharged state. The main differences arise from a decrease in the interatomic distances caused by the oxidation of V and removal of Li. Hence, the α-$NaFeO_2$-like Li_xVO_2 structure is retained and the material does not transform back to the rutile structure in line with the case of rutile TiO_2.[5,6] This is evidenced by the correlations at ~3.5 and 5.1–5.5 Å from the V–V in corner sharing $[VO_6]$ octahedra not reappearing upon charge (also see Supporting Information Figure S5, which compares the PDF of the pristine, chemical lithiated, discharged, and charged states). Despite the similarity between the discharged and charges state, some minor albeit important differences are noticed. The correlations at ~2.9, ~5.1, and 5.8 Å have a higher intensity in the discharged state, which is indicative of V on the Li-positions in the α-$NaFeO_2$-like Li_xVO_2 structure. The fade of

these correlations and the increase in intensity at ~6.2 Å indicate that the V on the Li-positions in the interlayer space migrate to the V-layers upon charge (see also calculated PDF in the Supporting Information Figure S4). The migration is likely enabled by the reduction in the ionic radius upon oxidation from V^{3+} to V^{4+}. Whether V remains within the V-layers upon repeated cycling will require further studies.

Based on the observations, it appears that Li-ion intercalation is the driver for the transition from the monoclinic rutile-like to the layered α-$NaFeO_2$-like Li_xVO_2 structure. As mentioned, when the (Li + V)/O ratio goes toward one, the rutile-like structure approaches a NiAs structure, which is generally not observed for metal oxides. The nature of the transition is likely linked to the ionic radius of Li^+ (90 pm), as this determines the strain induced by intercalation. To the best of our knowledge, Na-ion intercalation in $VO_2(M)$ has not been reported. This may be due to difficulties in intercalating the larger Na^+ ion. However, this would make for an interesting comparison. In contrast, hydrogenation of VO_2 materials has been widely explored,[31] which can be viewed as intercalation of H^+ ions. In studies specifically on monoclinic $VO_2(M)$,[32,33] they report that hydrogenation only induced minor structural changes, that is, the rutile-like structure is retained even as the (H + V)/O ratio in H_xVO_2 goes toward one. One study[32] even indicates that the monoclinic distortion diminishes. This underlines the point of the effect of the size of the intercalated ion.

CONCLUSIONS

The structural changes occurring during lithium insertion and extraction in a monoclinic distorted rutile $VO_2(M)$ LIB cathode were studied by using galvanostatic cycling, PXRD, and TXS-PDF. The phase of interest, $VO_2(M)$, was obtained *via* solvothermal synthesis followed by a solid-state treatment to yield the desired phase. During the first discharge, the rutile $VO_2(M)$ structure first accepts Li-ions *via* a solid solution reaction forming $Li_xVO_2(M)$ observed by *operando* PXRD and Rietveld refinement as changes to the unit cell parameters. Upon insertion of ~0.3 Li, the Bragg reflections become increasingly diffuse, and between 0.4 and 0.5 Li the Rietveld refinement fails due to loss of crystallinity. PDF analysis reveals that at this stage, $Li_xVO_2(M)$ transforms to a highly disordered layered α-$NaFeO_2$-like Li_xVO_2 structure along with a minor amount of a columbite-like structure. This resembles the case of rutile TiO_2 and suggests that this is a general behavior of rutile oxides because Li-ion intercalation results in formation of a NiAs structure, which is generally not stable for oxides. However, the Li-limit for the structural reconstruction into the ccp α-$NaFeO_2$-like appears to depend on the nature of the transition metal. Furthermore, this study indicates that in the α-$NaFeO_2$-like Li_xVO_2 structure forming during discharge, some V remains in the interlayer space (Li-positions) but migrates to the V-layers upon oxidation during the subsequent charge.

ASSOCIATED CONTENT

Supporting Information

The Supporting Information is available free of charge at https://pubs.acs.org/doi/10.1021/acsomega.4c02839.

> Rietveld fit of first *operando* PXRD scan, *Operando* PDF and galvanostatic dis-/charge curve, Le Bail fit of lithiated $VO_2(M)$, compare PDF with and without V migration, comparing PDF from pristine, discharged, charged, and chemical lithiated, Results from Rietveld on pristine material, results from PDF fit of pristine material, results from PDF fit (α-$NaFeO_2$-like and columbite) of the chemical lithiated sample, results from PDF fit (α-$NaFeO_2$-like) of the chemical lithiated sample (PDF)

AUTHOR INFORMATION

Corresponding Author

Dorthe B. Ravnsbæk − *Center for Integrated Materials Research, Department of Chemistry, Aarhus University, 8000 Aarhus C, Denmark;* orcid.org/0000-0002-8172-3985; Email: dorthe@chem.au.dk

Author

Morten Johansen − *Center for Integrated Materials Research, Department of Chemistry, Aarhus University, 8000 Aarhus C, Denmark;* orcid.org/0000-0002-9860-718X

Complete contact information is available at: https://pubs.acs.org/10.1021/acsomega.4c02839

Notes

The authors declare no competing financial interest.

ACKNOWLEDGMENTS

REFERENCES

(1) Christensen, C. K.; Henriksen, C.; Ravnsbæk, D. B. Nye materialer til fremtidens genopladelige batterier: Et kig ind i batteriets atomare verden. *Dan. Kemi* **2015**, *96*, 18−21.

(2) *World Energy Outlook 2021*; International Energy Agency, 2021.

(3) Andersen, B. P.; Ravnsbæk, D. B. Fremtidens Bæredygtige Batterier. *Dan. Kemi* **2022**, *103*, 12−16.

(4) Lee, J.; Urban, A.; Li, X.; Su, D.; Hautier, G.; Ceder, G. Unlocking the Potential of Cation-Disordered Oxides for Rechargeable Lithium Batteries. *Science* **2014**, *343* (6170), 519−522.

(5) Christensen, C. K.; Ravnsbæk, D. B. Understanding disorder in oxide-based electrode materials for rechargeable batteries. *JPhys Energy* **2021**, *3* (3), 031002.

(6) Christensen, C. K.; Mamakhel, M. A. H.; Balakrishna, A. R.; Iversen, B. B.; Chiang, Y. M.; Ravnsbaek, D. B. Order-disorder transition in nano-rutile TiO2 anodes: a high capacity low-volume change Li-ion battery material. *Nanoscale* **2019**, *11* (25), 12347−12357.

(7) Uchaker, E.; Zheng, Y. Z.; Li, S.; Candelaria, S. L.; Hu, S.; Cao, G. Z. Better than crystalline: amorphous vanadium oxide for sodium-ion batteries. *J. Mater. Chem. A* **2014**, *2* (43), 18208−18214.

(8) Chae, O. B.; Kim, J.; Park, I.; Jeong, H.; Ku, J. H.; Ryu, J. H.; Kang, K.; Oh, S. M. Reversible Lithium Storage at Highly Populated Vacant Sites in an Amorphous Vanadium Pentoxide Electrode. *Chem. Mater.* **2014**, *26* (20), 5874−5881.

(9) Munoz-Paez, A. Transition Metal Oxides: Geometric and Electronic Structures: Introducing Solid State Topics in Inorganic Chemistry Courses. *J. Chem. Educ.* **1994**, *71* (5), 381.

(10) Wang, H.; Jang, Y.-I.; Huang, B.; Sadoway, D. R.; Chiang, Y.-M. Electron microscopic characterization of electrochemically cycled LiCoO2 and Li(Al,Co)O2 battery cathodes. *J. Power Sources* **1999**, *81−82*, 594−598.

(11) Xu, C.; Reeves, P. J.; Jacquet, Q.; Grey, C. P. Phase Behavior during Electrochemical Cycling of Ni-Rich Cathode Materials for Li-Ion Batteries. *Adv. Energy Mater.* **2021**, *11* (7), 2003404.

(12) Zhuang, D.; Bazant, M. Z. Theory of Layered-Oxide Cathode Degradation in Li-ion Batteries by Oxidation-Induced Cation Disorder. *J. Electrochem. Soc.* **2022**, *169* (10), 100536.

(13) Li, J.; Liang, G.; Zheng, W.; Zhang, S.; Davey, K.; Pang, W. K.; Guo, Z. Addressing cation mixing in layered structured cathodes for lithium-ion batteries: A critical review. *Nano Mater. Sci.* **2023**, *5* (4), 404−420.

(14) Galy, J.; Miehe, G. Ab initio structures of (M2) and (M3) VO2 high pressure phases. *Solid State Sci.* **1999**, *1* (6), 433−448.

(15) Andersson, G.; Parck, C.; Ulfvarson, U.; Stenhagen, E.; Thorell, B. Studies on Vanadium Oxides. II. The Crystal Structure of Vanadium Dioxide. *Acta Chem. Scand.* **1956**, *10*, 623−628.

(16) Housel, L. M.; Quilty, C. D.; Abraham, A.; Tang, C. R.; McCarthy, A. H.; Renderos, G. D.; Liu, P.; Takeuchi, E. S.; Marschilok, A. C.; Takeuchi, K. J. Investigation of Conductivity and Ionic Transport of VO2(M) and VO2(R) via Electrochemical Study. *Chem. Mater.* **2018**, *30* (21), 7535−7544.

(17) Castro-Pardo, S.; Puthirath, A. B.; Fan, S.; Saju, S.; Yang, G.; Nanda, J.; Vajtai, R.; Tang, M.; Ajayan, P. M. VO2 phase change electrodes in Li-ion batteries. *J. Mater. Chem. A* **2024**, *12* (5), 2738−2747.

(18) Munozrojas, D.; Baudrin, E. Synthesis and electroactivity of hydrated and monoclinic rutile-type nanosized VO2. *Solid State Ionics* **2007**, *178* (21−22), 1268−1273.

(19) Tian, J.; Liu, F.; Shen, C.; Zhang, H.; Yang, T.; Bao, L.; Wang, X.; Liu, D.; Li, H.; Huang, X.; et al. A new route to single crystalline vanadium dioxide nanoflakes via thermal reduction. *J. Mater. Res.* **2007**, *22* (7), 1921−1926.

(20) Park, S.; Lee, C. W.; Kim, J.-C.; Song, H. J.; Shim, H.-W.; Lee, S.; Kim, D.-W. Heteroepitaxy-Induced Rutile VO2 with Abundantly Exposed (002) Facets for High Lithium Electroactivity. *ACS Energy Lett.* **2016**, *1* (1), 216−224.

(21) Xiong, F.; Tao, H.; Yue, Y. Role of Amorphous Phases in Enhancing Performances of Electrode Materials for Alkali Ion Batteries. *Front. Mater.* **2020**, *6*, 328.

(22) Corr, S. A.; Grossman, M.; Shi, Y.; Heier, K. R.; Stucky, G. D.; Seshadri, R. VO2(B) nanorods: solvothermal preparation, electrical properties, and conversion to rutile VO2 and V2O3. *J. Mater. Chem.* **2009**, *19* (25), 4362.

(23) Basham, M.; Filik, J.; Wharmby, M. T.; Chang, P. C.; El Kassaby, B.; Gerring, M.; Aishima, J.; Levik, K.; Pulford, B. C.; Sikharulidze, I.; et al. Data Analysis WorkbeNch (DAWN). *J. Synchrotron Radiat.* **2015**, *22* (3), 853−858.

(24) Rodríguez-Carvajal, J. Recent advances in magnetic structure determination by neutron powder diffraction. *Phys. B* **1993**, *192* (1−2), 55−69.

(25) Rodriguez-Carvajal, J. Recent developments of the program FULLPROF, commission on powder diffraction. *IUCr Newsl.* **2001**, *26*, 12−19.

(26) Juhás, P.; Davis, T.; Farrow, C. L.; Billinge, S. J. L. PDFgetX3: a rapid and highly automatable program for processing powder diffraction data into total scattering pair distribution functions. *J. Appl. Crystallogr.* **2013**, *46* (2), 560−566.

(27) Farrow, C. L.; Juhas, P.; Liu, J. W.; Bryndin, D.; Božin, E. S.; Bloch, J.; Proffen, T.; Billinge, S. J. L. PDFfit2 and PDFgui: computer programs for studying nanostructure in crystals. *J. Phys.: Condens. Matter* **2007**, *19* (33), 335219.

(28) Momma, K.; Izumi, F. VESTA 3 for three-dimensional visualization of crystal, volumetric and morphology data. *J. Appl. Crystallogr.* **2011**, *44* (6), 1272−1276.

(29) Liu, C.; Neale, Z. G.; Cao, G. Understanding electrochemical potentials of cathode materials in rechargeable batteries. *Mater. Today* **2016**, *19* (2), 109−123.

(30) Kulish, V. V.; Koch, D.; Manzhos, S. Ab initio study of Li, Mg and Al insertion into rutile VO2: fast diffusion and enhanced voltages for multivalent batteries. *Phys. Chem. Chem. Phys.* **2017**, *19* (33), 22538−22545.

(31) Kumar, A.; Kumar, A.; Kandasami, A.; Singh, V. R. A Comprehensive Review on Synthesis, Phase Transition, and Applications of VO2. *J. Supercond. Nov. Magnetism* **2024**, *37*, 475−498.

(32) Chen, S.; Wang, Z.; Ren, H.; Chen, Y.; Yan, W.; Wang, C.; Li, B.; Jiang, J.; Zou, C. Gate-controlled VO2 phase transition for high-performance smart windows. *Sci. Adv.* **2019**, *5*, No. eaav6815.

(33) Pofelski, A.; Jia, H.; Deng, S.; Yu, H.; Park, T. J.; Manna, S.; Chan, M. K. Y.; Sankaranarayanan, S. K. R. S.; Ramanathan, S.; Zhu, Y. Subnanometer Scale Mapping of Hydrogen Doping in Vanadium Dioxide. *Nano Lett.* **2024**, *24*, 1974−1980.